Journal of Alloys and Compounds 1013 (2025) 178475

Contents lists available at ScienceDirect

Journal of Alloys and Compounds

journal homepage: www.elsevier.com/locate/jalcom

# Ultra-exclusive selectivity for the detection of formaldehyde in laser-induced ZnO mesh sensor with few-nanometer pores

Seung-Jo Kang [a,b], Jihyun Lee [a], James Jungho Pak [b,*], Yu Jin Kim [a,c,**], Wooyoung Lee [a,*]

[a] Department of Materials Science and Engineering, Yonsei University, 50 Yonsei-ro, Seodaemun-gu, Seoul 03722, Republic of Korea
[b] School of Electrical Engineering, Korea University, 145 Anam-ro, Seongbuk-gu, Seoul 02841, Republic of Korea
[c] KIURI Institute, Yonsei University, 50 Yonsei-ro, Seodaemun-gu, Seoul 03722, Republic of Korea

ARTICLE INFO

*Keywords:*
ZnO gas sensor
Formaldehyde gas sensor
Laser-induced ZnO
ZnO mesh structure
Formaldehyde selectivity

ABSTRACT

Formaldehyde is classified as a Group 1 biological agent that is "carcinogenic to humans." A gas sensor can be developed as a chemiresistive device with rapid response, outstanding sensitivity, reproducibility, and excellent selectivity for the detection of formaldehyde, providing a crucial pathway to protect human health in formaldehyde-rich environments. To this end, we designed a formaldehyde gas sensor that demonstrates ultra-exclusive selectivity, including a superior sensing response of 6682.8 at 10 ppm formaldehyde and 1687.6 for the optimized sensor with reasonable response (2.96 s) and recovery (46.2 s) times, based on a ZnO mesh structure. The sensor was fabricated using a rapid 1-min $CO_2$ laser process, forming a ZnO precursor into a mesh structure with few nanometer-sized pores between ZnO crystal domains. The small kinetic size (2.43 Å) and large dipole moment (2.30 D) of formaldehyde allow for effective adsorption and good permeability within these pores, providing exceptional selectivity. Other gases such as acetone, styrene, and $CO_2$ showed significantly lower responses, confirming the sensor's selectivity for formaldehyde. Oxygen vacancies, which increased with laser power (up to 38 % at 4 W), played a crucial role in enhancing the interaction between formaldehyde and the ZnO surface, contributing to the sensor's high sensitivity and efficiency. Additionally, the sensor exhibited excellent long-term stability, with only a 15 % reduction in response over 7 weeks of continuous operation at 400°C. The sensor also showed a linear correlation ($R^2 = 0.999$) across a range of formaldehyde concentrations (0.01 ppm to 10 ppm), with a low detection limit (LOD) of ~0.1 ppm, making it suitable for detecting even trace amounts of formaldehyde. This ultra-exclusive formaldehyde gas sensor design offers a promising strategy for air quality monitoring in both indoor and outdoor environments, with significant potential for public health protection.

## 1. Introduction

Formaldehyde, a simple aldehyde, has been widely used in the synthesis of bakelite as a plastic material, disinfectant, and building material. In particular, as a toxic gas, it causes sick building syndrome and is a main issue to occur atopic dermatitis. It becomes a destroyer that causes ecological environmental problems and biological disturbance, it is thereby classified as a Group 1 human carcinogen [1–3]. Chemically understanding this pollutant and its selective detection is seriously important to defend human health in life-threatening environments.

The highly selective detection of formaldehyde, especially in air pollutants, is still a longstanding challenge. However, it is feasible in several strategies. In terms of molecular formation, it is one of the smallest molecules with a kinetic diameter of 2.43 Å in size [4].

Formaldehyde molecules have competitiveness of gas adsorption in the finite area of the sensing materials, bringing an idea that an increase in the surface area of the materials allows high adsorption response of the molecules [5–9]. In this case, a few nanometer-sized structures [5–7], the formation of the porous or hollow shape [10,11], generation of nano-gap or -crack [12], or introduction of embossing structure [13], etc., can be suggested. In the chemical structure perspective, the molecule has the effectiveness of chemisorption with adsorbed oxygen ion species on the surface of air-exposed sensing materials. It means that semiconducting metal oxide, in particular n-type semiconductor, is a great candidate to generate the ion species in the oxygen-deficient crystal structure by trapping electrons released from the conduction

* Corresponding authors.
** Correspondence to: Department of Materials Science and Engineering and KIURI Institute, Yonsei University, Seoul, Republic of Korea.
*E-mail addresses:* pak@korea.ac.kr (J.J. Pak), yujin.kim@yonsei.ac.kr (Y.J. Kim), wooyoung@yonsei.ac.kr (W. Lee).

https://doi.org/10.1016/j.jallcom.2025.178475
Received 20 July 2024; Received in revised form 30 November 2024; Accepted 2 January 2025
Available online 5 January 2025

band of the metal oxide [14]. Therefore, a zinc oxide (ZnO)-based chemiresistor device with few nanometer-sized pores in the ZnO structure would be a superior gas sensor with high selectivity toward formaldehyde.

Many studies regarding formaldehyde gas sensors with ZnO semiconductors have mainly focused on metal-incorporated ZnO (metal: Au, Ag, Ni, or Al) [15–18], the materialization of ZnO nanocomposites with other oxide materials [19,20], or a polymer hybrid structure [21]. Applications for pure ZnO structure in the sensors have been rarely reported, two research show a 5–10 μm-sized agglomeration consisting of ZnO nanorods [22] and porous ZnO nanoplates with a pore diameter of ca. 100 nm [23], respectively.

In this work, we developed a formaldehyde chemiresistor sensor that has a ZnO mesh structure with few nanometer-sized pores. Laser irradiation enables a ZnO precursor to design the mesh structure that has few nanometer-sized pores between ZnO crystal domains. The structure allows effective gas adsorption and the generation of sufficient oxygen ion species on the surface, facilitating efficient chemical interaction with the formaldehyde target gas. It thereby leads to the detection toward formaldehyde in an excellent sensing response (over 6682 value to 10 ppm formaldehyde), corresponding to ultra-exclusive selectivity manner.

Through the development of the ZnO mesh structure with few nanometer-sized pores, we finally realized an ideal ZnO sensor device toward formaldehyde in indoor and outdoor air monitoring.

## 2. Experimental section

### 2.1. Preparation of a ZnO metallo-hydrogel precursor solution

Zinc nitrate hexahydrate ($Zn(NO_3)_2{\cdot}6H_2O$, reagent grade 98 %) and gelatin (type A from porcine, gel strength 300) were purchased from Sigma-Aldrich. The chemicals were received and used directly without further purification. A $Zn(NO_3)_2{\cdot}6H_2O$ solution (2 mol/kg) was prepared by dissolving in deionized water (di-water) at 80 °C. Gelatin of 20 wt% was added to the $Zn(NO_3)_2{\cdot}6H_2O$ solution, and then the mixture was blended for 10 min at 800 rpm using a high-torque overhead stirrer (WiseStir® HT-50T). During blending the mixture, high-density bubbles were generated. To remove the bubbles, it was sealed to prevent air interaction and heated at 80 °C for 36 h. The bubbles in the solution disappeared, and a transparent ZnO precursor solution was obtained.

### 2.2. Fabrication of the laser-induced ZnO mesh sensor devices

Interdigitated electrodes (IDEs) that were composed of Cr and Pt with a 50 nm and 100 nm thickness, respectively, were patterned on a $SiO_2$/Si substrate (8.5 mm × 8.5 mm) by the liftoff method [24]. The $SiO_2$/Si substrate was cleaned by ultrasonication in acetone and isopropyl alcohol for each 15 min. To pattern the electrodes by the lift-off method, the LOR 5 A resist (purchased from AllforLab, Inc.) was spin-coated onto the cleaned substrate at 3000 rpm for 45 s. After the LOR 5 A layer was solidified at 190 ºC for 5 min, AZ GXR-601 (photoresist / viscosity 14 CP, purchased from NM Tech.) was spin-coated onto the LOR 5 A layer at 3000 rpm for 30 s. A soft bake was sequentially performed at 110 ºC for 1 min. The resist layer was treated from a UV exposure (15 s) with a patterned mask, and then the substrate was soaked into a developer solution (AZ 300 MIF, purchased from Sigma-Aldrich) for 11 s without a post-exposure bake (PEB) process. The Cr/Pt electrode was thermally deposited, and the substrate was soaked in acetone to remove the resist layer. The IDEs with a 10 μm gap can be an active site for the deposition of ZnO precursor, whereas the non-active area was covered by polyimide (PI) tape as passivation. On the active site, the ZnO precursor solution was spincoated for 30 s at 1000 rpm, and the ZnO precursor film was exposed to $CO_2$ laser irradiation (a scan speed of 126 mm $s^{-1}$) with different laser power (0, 1, 2, 3, and 4 W in this work) for ~ 1 min. Finally, the PI passivation tape was removed, and the laser-induced ZnO mesh sensor was fabricated.

### 2.3. Gas sensing measurement of the laser-induced ZnO mesh sensor devices

The sensing abilities of the laser-induced ZnO mesh sensors were evaluated using a customized sensing measurement system with four-channel test equipment. It has a tube furnace (quartz tube with a 25∅) chamber equipped with a gas flow system (the gas line has a 6∅), which is connected to mass flow controllers (MFCs) and gas cylinders. For the selective sensing test, all gases (formaldehyde (HCHO – dry gas, concentration of 10.8 μmol/mol with $N_2$ balance gas), acetone (concentration of 10 μmol/mol with $N_2$ balance gas), styrene (concentration of 10 μmol/mol with $N_2$ balance gas), carbon dioxide ($CO_2$ – dry gas, concentration of 197.8 μmol/mol with dry air balance gas), ammonia ($NH_3$ – dry gas, concentration of 10 μmol/mol with dry air balance gas), nitrogen dioxide ($NO_2$ – dry gas, concentration of 49.2 μmol/mol with dry air balance gas), and nitric oxide (NO – dry gas, concentration of 103.7 μmol/mol with $N_2$ balance gas), acetaldehyde (dry gas, concentration of 10.1 μmol/mol with $N_2$ balance gas), and ethanol (dry gas, concentration of 10.1 μmol/mol with $N_2$ balance gas)) were used with a concentration of 10 ppm that was diluted to the standard gas (80 % nitrogen and 20 % oxygen) with dry air. In the gas sensitivity test, the concentration of the formaldehyde ranged from 0.01 ppm to 10 ppm. The specific concentrations of the target gas were also diluted to the standard gas with dry air. For both gas testing cases, specific concentrations of the target gas and the standard gas with dry air as the balance gas were injected into the chamber at a constant flow rate of 1000 sccm. The operating temperature (300 ºC – 500 ºC) of the chemiresistive sensor was provided and adjusted using a temperature controller embedded in the tube furnace. The temperature controller utilized a typical algorithm that incorporated feedback from the temperature sensor with an error range of ± 0.5 °C. The electrical sensing resistance was measured using a nanovoltmeter (Keithley 2182) at a constant current of 1 μA (a DC current source - Keithley 6220) with a time interval of 1 s under an LabView environment, which controlled all the accessories.

### 2.4. General characterization

Feld-emission scanning electron microscopy (FE-SEM) images including cross-sectional results of the laser power-dependent ZnO mesh films were measured using a JEOL-6701F instrument. The internal crystal morphologies of the ZnO mesh structures were confirmed by transmission electron microscopy (TEM) which was operated at an acceleration voltage of 200 kV (JEM -ARM 200F, JEOL Ltd). The crystal lattice phases of the mesh structure were evaluated by X-ray diffraction (XRD) (Cu Kα radiation, $\lambda = 1.541$ Å) (Ultima IV/ME 200DX, Rigaku). Ex-situ temperature-dependent XRD results were measured by thermal-annealing for each sample at 45 min with the same Rigaku XRD instrument. X-ray photoelectron spectroscopy (XPS) measurement was performed with a K-alpha system (Thermo Fisher Scientific) using a monochromatic Al Kα irradiation (1486.6 eV) to investigate the surface composition and chemical states of the laser-induced ZnO mesh samples. The electronic spin states and surface structures were examined using an electron paramagnetic resonance (EPR) spectrometer (EMXplus-9.5/12/P/L, Bruker) operating at an X-band frequency (f ≈ 9.774 GHz). The distribution of pore diameters was measured using a porosimeter (Quantachrome PM33GT). The surface area including pore volume was investigated by Brunauer-Emmett-Teller (BET) method from the desorption branch data of nitrogen adsorption isotherm at 77.4 K with an Autosorb IQ (Quantachrome).

## 3. Results and discussion

A speedy-fabricated ZnO mesh sensor can be designed by $CO_2$ laser irradiation. Fig. 1a shows the overall design of the chemiresistive device

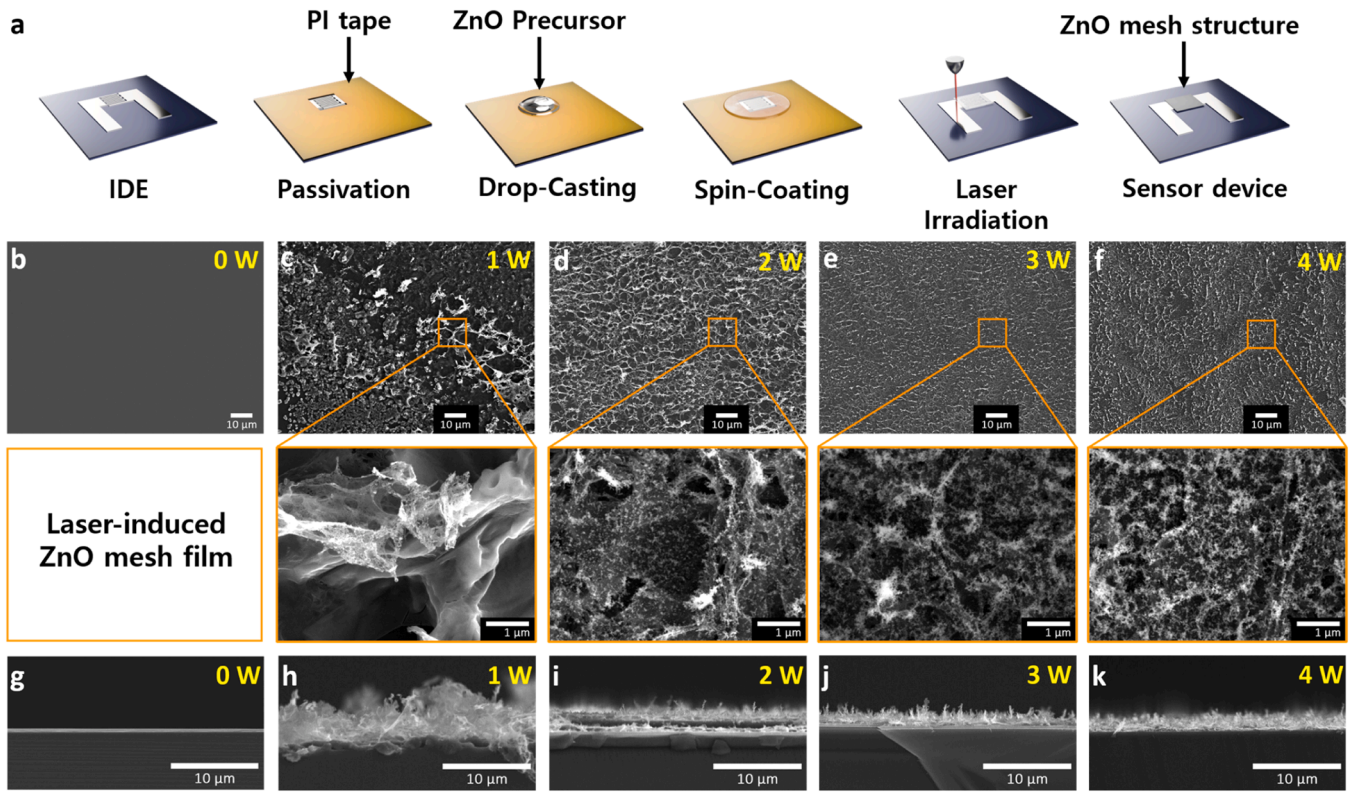


**Fig. 1.** (a) A step scheme of the fabrication of a laser-induced ZnO gas sensor (IDE: interdigited electrodes). Surface morphological structures of laser-induced ZnO mesh films in laser power dependence: (b-f) SEM images, corresponding to (g-k) cross-sectional SEM results (b and g – 0 W, c and h – 1 W, d and i – 2 W, e and j – 3 W, and f and k – 4 W).

that designates an extremely selective formaldehyde sensor (details are described in the Experimental section). A ZnO solution is exposed to $CO_2$ laser irradiation for ~ 1 min. The strong power of the laser enables to spark instantaneous high temperature (~ 2000 K can be reached in a few seconds), which allows the generation of ZnO crystals in a mesh structure from the precursor.

We expected that the ZnO mesh structure has a laser power-dependent effect. Indeed, depending on the laser power, the morphological ZnO structures were varied; Fig. 1b-f exhibits FE-SEM images. Each orange box in the Figure below shows an enlarged view. A pure structure without morphological feature was shown in the as-cast ZnO film (0 W, Fig. 1b).

Upon laser irradiation, however, a thin foil sheet with over 1 μm-sized holes was observed in the ZnO film processed with a 1 W power (Fig. 1c). As an increase of the laser power to 2 W (Fig. 1d), the ZnO foil sheet was changed to a mesh structure that has aggregated particles on the surface with hundreds of nanometers in size (Fig. 1d). For stronger power conditions at 3 W (Fig. 1e) and 4 W (Fig. 1f), the ZnO films keep the mesh structure, however, hundred nanometer-sized particles that were shown in the 2 W laser condition mostly disappeared. It suggests that ZnO crystals might be formed in the mesh structure without non-reactive particle aggregation. In comparison between 3 W and 4 W conditions, the 4 W laser-induced ZnO film showed a closer mesh structure with ca. 200 nm-sized holes (the 3 W laser-induced ZnO film has over 650 nm-sized holes). The cross-sectional SEM images show the growth of the ZnO crystals in the mesh film in detail (Fig. 1g-k). Beyond the foil sheet that is shown at the 1 W laser condition (Fig. 1h), we found that the ZnO crystals were randomly grown with a spark shape in the mesh structure (Fig. 1i). However, the spark formation gradually decreased as a function of laser power (Fig. 1j-k), indicating that the aggregated formation in Fig. 1d might be from the ZnO spark crystals, and thus higher laser power allows the formation of ZnO crystal domains in the mesh structure without aggregated ZnO spark feature.

To understand the internal structure of the ZnO crystals in the mesh film, we measured TEM images. Fig. 2 exhibits laser power-dependent ZnO structures, and higher magnified TEM results were highlighted as an orange box. As consistent with the surface morphology of Fig. 1c, the aggregated ZnO formation was observed in the 1 W laser-induced ZnO mesh structure (Fig. 2b). It indicates that non-reactive particle aggregation in the synthesis of ZnO crystal is shown in the internal mesh structure. As an increase of the laser power to more than 2 W, a specified structure, i.e., the aggregated particle formation, was rarely revealed, whereas a nanosheet morphology was observed (Fig. 2c for 2 W, Fig. 2d for 3 W, and Fig. 2e for 4 W laser power condition). When a sectional point in the sheet is focused, we understand that the sheet has a hexagonal wurtzite structure from the ZnO crystal (yellow marks) [25]: (100) lattice plane with a spacing of 0.28 nm, (002) lattice plane with a spacing of 0.26 nm, and (110) lattice plane with a spacing of 0.25 nm. It demonstrates that ZnO crystals are randomly synthesized without specific features in the mesh film and they are uniformly dispersed in the mesh structure in the laser power condition over 2 W.

From the surface and internal morphologies, we understand that 1) higher laser power, in particular over 2 W condition, allows the generation of ZnO crystals in the mesh film with a more compact formation and 2) the crystals are more evenly dispersed in the mesh structure as the nanosheet formation. All laser-induced ZnO mesh structures present ZnO crystal phases including ZnO aggregation in the morphologies, however, the degree of the ZnO crystallinity has a laser power dependency; XRD data of Fig. 2f proves this comment (a highlighted figure that has an X-axis range of 25 ° - 45 ° was displayed from a blue dash box in Fig. 2f). In the ZnO precursor state without laser irradiation (0 W laser power), two-theta peaks at 23.0°, 30.5°, and 53.3° were observed, corresponding to α-$Zn(OH)_2$ (JCPDS No. 041–1359) and λ-$Zn(OH)_2$ (JCPDS No. 038–0356). At 1 W laser power, similar diffraction peaks appeared, indicating that neither the 0 W nor 1 W conditions provide enough energy for ZnO crystallization. However, at 2 W, the diffraction profile

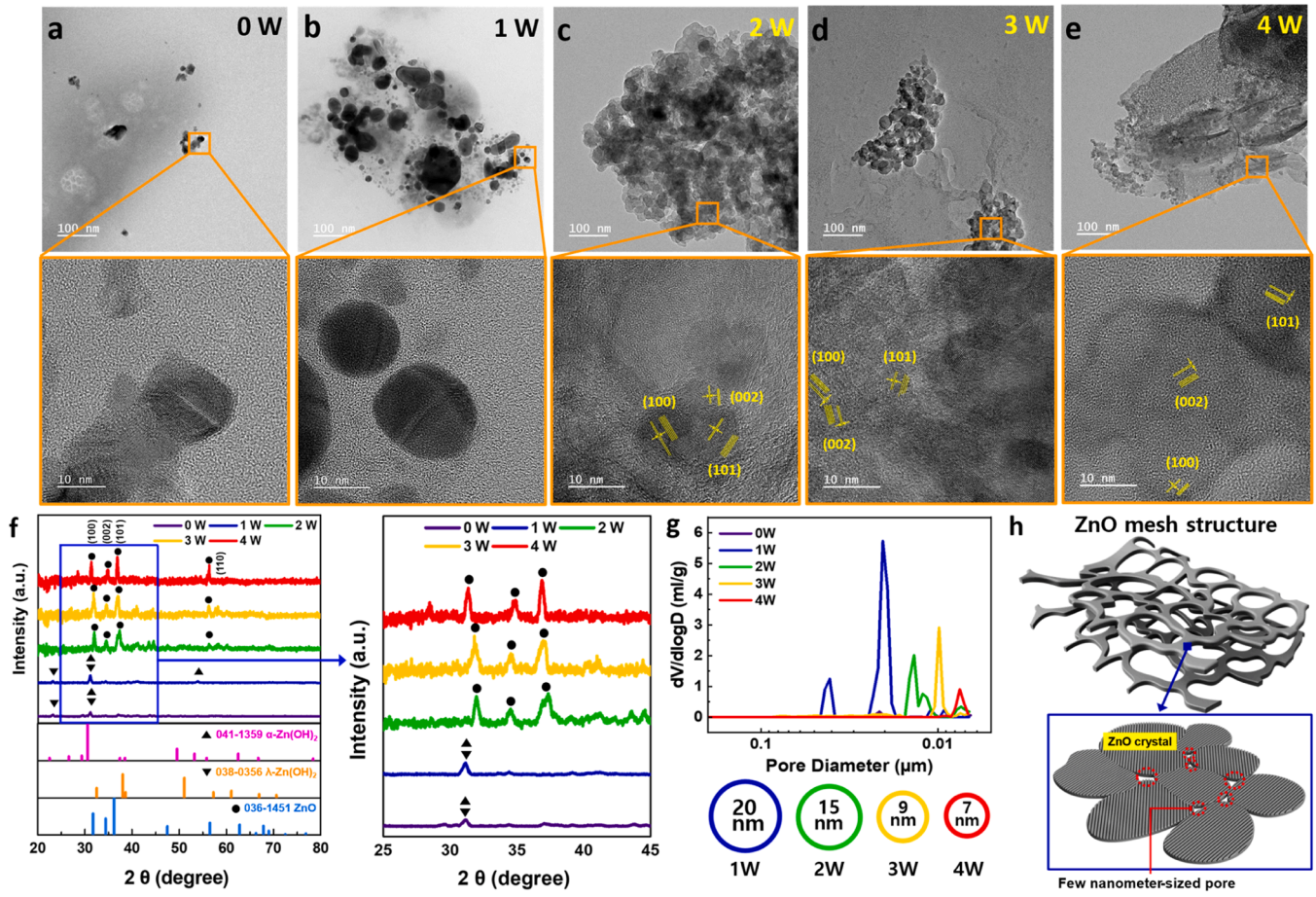


**Fig. 2.** Internal structures of laser-induced ZnO mesh films as a function of laser power: (a – e) TEM images, (f) XRD results, (g) pore size distributions, and (h) suggested ZnO mesh structure.

(green line) revealed the hexagonal wurtzite ZnO crystal (JCPDS No. 36–1451), as shown by the sharper peaks and increased intensity. For 3 W and 4 W, higher diffraction intensities at the same Bragg positions indicated a trend of increased crystallinity. The sharpening of peaks and reduction in broadening suggest larger crystallite sizes and less internal strain at higher powers. Using the Scherrer equation, it would be possible to calculate crystallite sizes, which would likely show increasing size with higher laser power. Furthermore, no secondary phases were observed at higher laser powers, demonstrating the removal of hydroxide impurities and the formation of phase-pure ZnO.Thus, the XRD results clearly show that higher laser power enhances both crystallinity and phase purity, resulting in well-formed ZnO crystals.

As a strategy in the design of the formaldehyde gas sensor, we argued that few nanometer sized pores in the sensing material lead to a superior selective sensor in the detection of formaldehyde. Thus, we investigated the distribution of pore diameters in the ZnO mesh structures. Fig. 2g describes the laser power dependent-distribution of pores in size, which was measured by a porosimeter. Stronger laser power provides smaller pores in the ZnO mesh structure; no pore at 0 W, 20 nm-sized pores in diameter at 1 W (majority, 40 nm-sized pores are minor), 15 nm-sized pores in diameter at 2 W, 9 nm-sized pores in diameter at 3 W, and 7 nm-sized pores in diameter at 4 W. This trend is similar results with previously reported papers using the $CO_2$ laser system [26,27] and demonstrates that the ZnO crystals are synthesized in the mesh structure with smaller pores between the crystal domains as an increase of the laser power. The 3 W or 4 W laser powers provide few nanometer-sized pores in the ZnO mesh structure, which might allow exclusive permeability for formaldehyde gas. The BET results support the distribution of pore diameters that the surface area including pore volume showed an increased trend as a function of laser power (Fig. S1). With the information on pore size in the morphological studies, therefore, we expect that the laser-induced ZnO mesh structure processed with higher laser power, in particular at 3 W or 4 W would provide excellent sensing performance, in particular for the formaldehyde selectivity. We suggest this ideal ZnO mesh structure as shown in Fig. 2h.

We investigated the surface composition and chemical states of elements on the laserinduced ZnO mesh films. From the XPS analysis, we understand that higher contents of oxygen vacancies are formed in the ZnO mesh structure that has a well-structured ZnO crystal framework. Fig. 3 displays the XPS spectra of the O 1 s state for the laser power-dependent ZnO mesh films (the full-scan spectra of Fig. S2 provide an involvement of Zn, O, N, and C elements). The O 1 s peaks are deconvoluted into three individual quasi-Gaussian peaks and they were centered at ~ 530.1, ~ 531.4, and ~ 532.4 eV (the 0 W laser power condition was excluded due to the non-synthesized ZnO crystal). The three peaks were determined to be O Lattice, O vacancy, and O chemisorbed, and the meaning of each peak corresponds to the following [28–30]: The O Lattice refers to $O^{2-}$ ions of Zn-O bonds in the ZnO crystal, which is shown as a low-energy curve (blue line). The O vacancy is attributed to the oxygen ions of $O^{-}$ or $O^{2-}$ in the oxygen-deficient regions in the ZnO framework (intermediate-energy curve, pink line). The O chemisorbed means the chemisorbed oxygen species e.g., $O^{-}$, $O^{2-}$ or OH groups, on the ZnO surface (high-energy curve, green line). Among the oxygen states, it is important to understand the O vacancy level because oxygen vacancies in the crystal donate electrons that are obtained from the conduction band of the ZnO semiconductor to adsorbed oxygen molecules, allowing chemical interactions of the molecules with a target gas [14,31]. In the curve of the O vacancy state, therefore, the

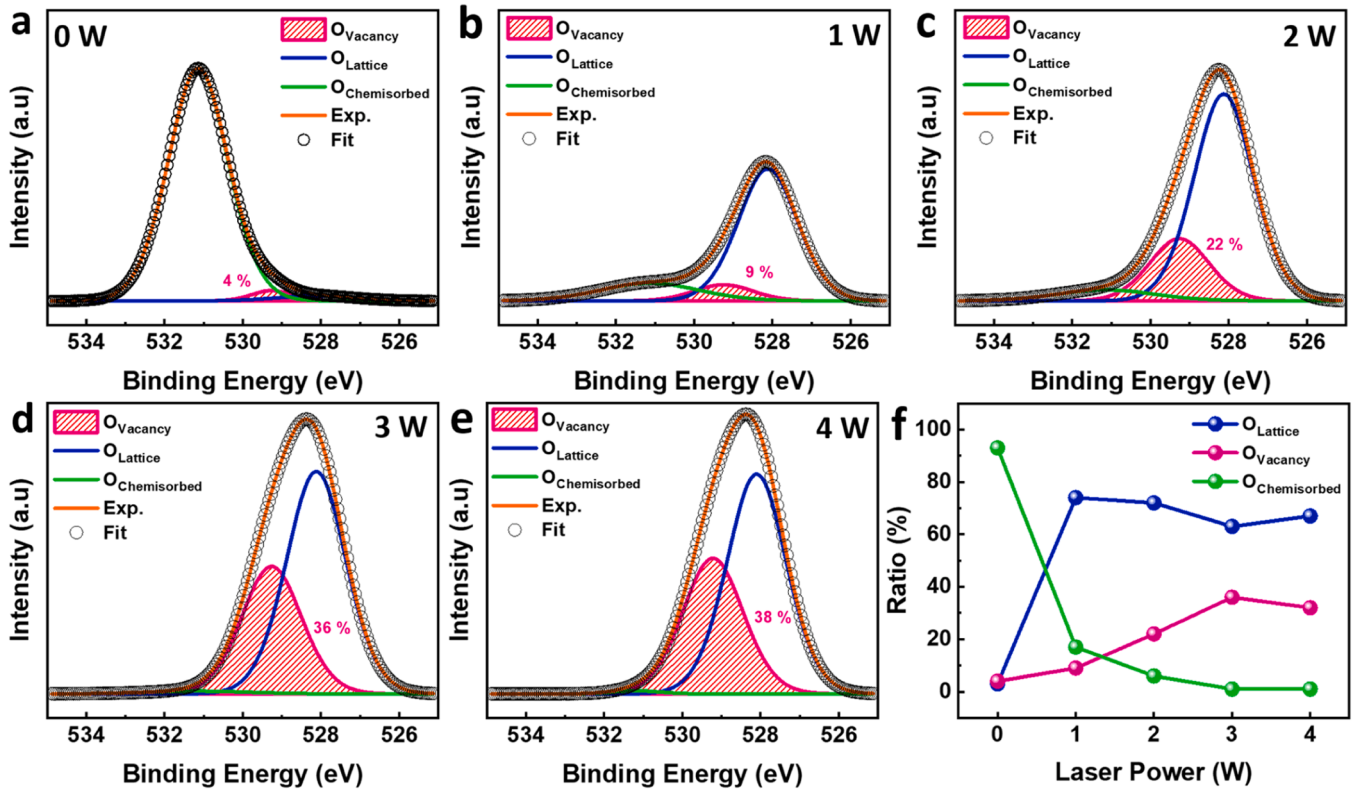


**Fig. 3.** XPS core-level spectra of O 1 s for the chemical state analysis of the surface on the laser-induced ZnO mesh structures depending on the laser power (a-e, 0 W – 4 W). (f) Trends of lattice oxygen (O Lattice), oxygen vacancy (O vacancy), and chemisorption of oxygen (O chemisorbed) depending on the laser power.

number of oxygen vacancies was estimated as a relative percentage of the area fraction (pink diagonal lines); ~ 9 % for 1 W (Fig. 3b), ~ 22 % for 2 W (Fig. 3c), 36 % for 3 W (Fig. 3d), and 38 % for 4 W (Fig. 3e). We find a gradually emerging trend as a function of laser power, which is shown in Fig. 3f. The trend indicates that higher laser power allows the formation of ZnO crystals with higher crystallinity in the mesh structure, more oxygen vacancies were generated in the crystals.

We investigated the electronic properties of the laser-induced ZnO mesh films using EPR spectroscopy. The EPR analysis provided insights into the oxygen vacancy sites in the ZnO structure by monitoring the behavior of unpaired electrons trapped within these vacancies. Fig. S3 displays the EPR spectra for the ZnO mesh films synthesized under varying laser powers. As shown in Fig. S3, the g-factor values exhibited a clear increasing trend with higher laser power, indicating the generation of a greater number of oxygen vacancies [32–34]. The g-factor, a parameter that reflects the interaction of unpaired electrons with the magnetic field, is directly related to the presence of oxygen vacancy sites. Higher g-factor values correspond to an increased density of unpaired electrons trapped in oxygen-deficient regions of the ZnO framework. This observation suggests that as the laser power used during ZnO synthesis increases, the rapid heating and cooling cycles promote the formation of oxygen vacancies, which serve as trapping sites for unpaired electrons. The data align with previous findings that demonstrated enhanced crystallinity and structural modifications with increased laser power. The higher density of oxygen vacancies at elevated laser powers further confirms the trend observed in XPS analysis, providing complementary evidence that laser power significantly influences the structural and electronic properties of ZnO mesh films. These vacancies are crucial for enhancing gas sensing performance by facilitating stronger adsorption and reaction dynamics with target gas molecules.

To investigate the effect of the ZnO mesh structure on a gas sensor, the gas-sensing characteristics were tested. The laser-induced ZnO mesh sensors were operated for the detection of 10 ppm formaldehyde at various temperatures ranging from 300 °C to 500 °C. All sensor devices showed an n-type oxide semiconductor behavior [35] and temperature dependent sensing resistance (Fig. 4a-e). All sensors exhibited a variation of initial resistance level in air ($R_a$) as a function of temperature. It is because of the change in the intrinsic properties of ZnO according to the oxygen molecules adsorbed on the surface when the ZnO is exposed to air [33]. In general, the chemisorbed oxygen species can be ionized to different chemical forms depending on the operating temperature [36, 37];

$$O_{2(ads)} + e^- \leftrightarrow O^-_{2(ads)}, \mathrm{T} < \quad 150 \quad ^\circ\mathrm{C} \tag{1}$$

$$O_{2(ads)} + e^- \leftrightarrow 2O^-_{(ads)}, \ 150 \quad ^\circ\mathrm{C} \leq \mathrm{T} \leq \quad 400 \quad ^\circ\mathrm{C} \tag{2}$$

$$O^-_{(ads)}, \quad + e^- \leftrightarrow O^{2-}_{(ads)}, \ \mathrm{T} > \quad 400 \quad ^\circ\mathrm{C} \tag{3}$$

Based on the 400 °C, the predominant adsorbed oxygen species are different, which causes one of the reasons for the change in the electrical resistance of n-type ZnO. In the selective resistance result at the operating temperature of 400 °C (Fig. 4f), we find that the $R_a$ level increases as an increase of the laser power in the ZnO mesh sensor with a basis of $R_a$ signal at the 0 W laser power. It means that a thicker electron depletion layer that generates more electrons is formed on the surface of ZnO with higher laser power [38], which has a larger possibility to interact with more chemisorbed oxygen molecules from the air, i.e., $O^-$ and $O^{2-}$ on the surface.

With the resistance concept, in the air environment, we thereby understand that the electrons are transferred from the conduction band of ZnO to the chemisorbed oxygen species, leading to an increase in both the energy potential barrier ($E_p$) and thickness of the electron depletion layer as the electron concentration decreases (Fig. 5a and 5c). In the formaldehyde condition, formaldehyde target molecules chemically interact with the chemisorbed oxygen molecules with the following

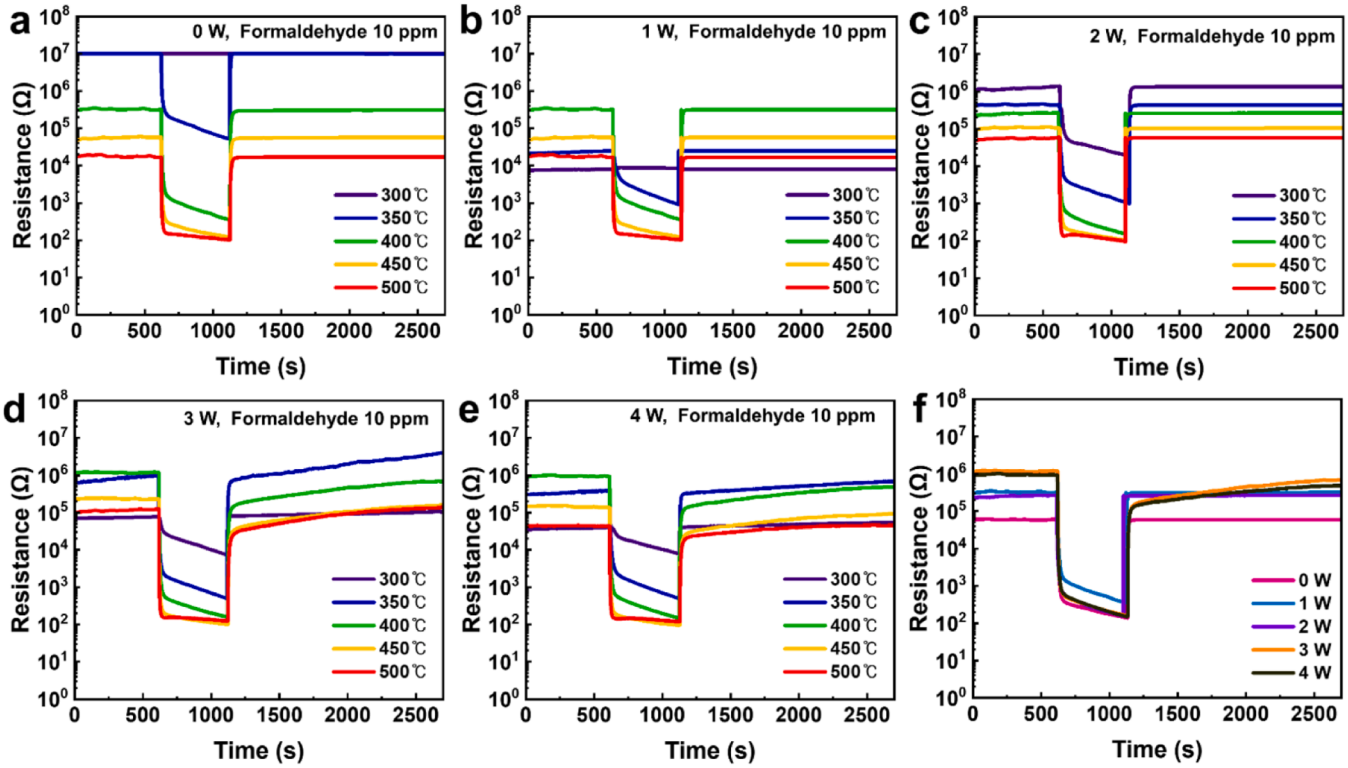


**Fig. 4.** Dynamic results for sensing resistance (formaldehyde 10 ppm) of the laser-induced ZnO mesh sensors prepared by laser power of (a) 0 W, (b) 1 W, (c) 2 W, (d) 3 W, and (e) 4 W. (f) Variation in the resistance at 400 ℃ measured by the laser-induced ZnO mesh sensors depending on the laser power.

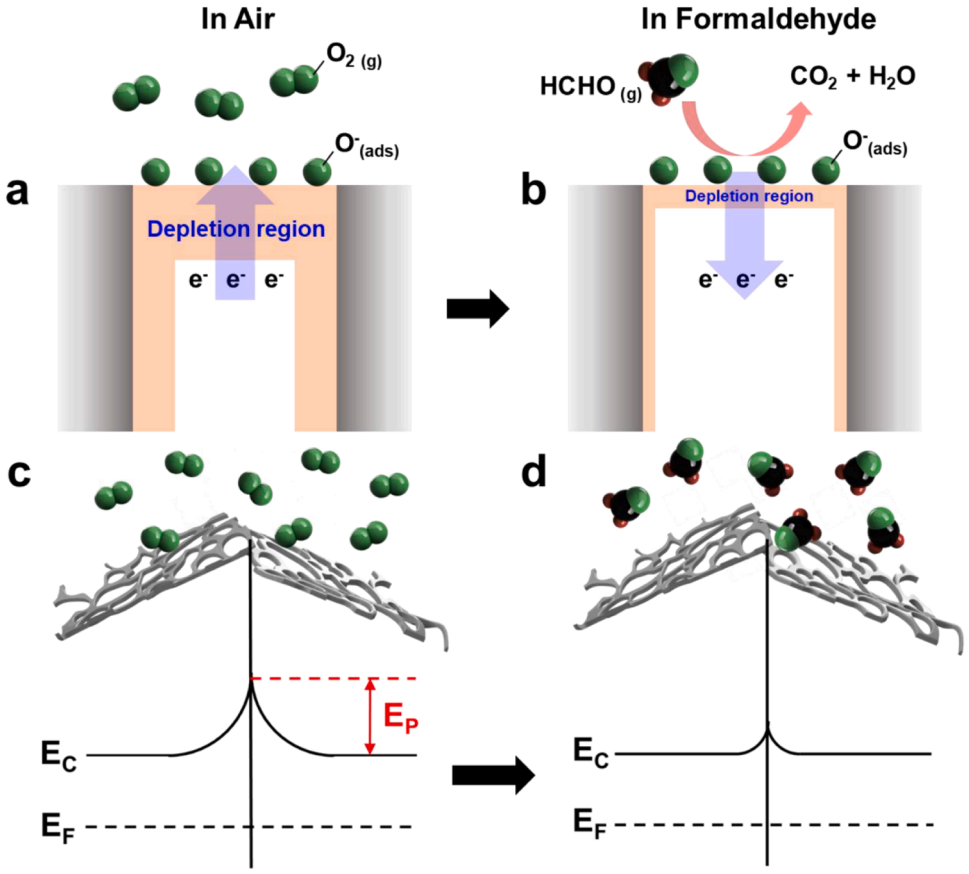


**Fig. 5.** Schematic illustrations of the gas sensing mechanism in air (a and c) and formaldehyde (b and d) environment. In Fig. c and d, the energy barrier potential (E p) is expressed with the conduction band level of E c and Fermi level of E F.

chemical reactions [39,40].

$$HCHO_{(g)} + 2O^{-}_{(ads)} \leftrightarrow H_2O + CO_2 + 2e^{-} \quad (4)$$

$$HCHO_{(g)} + 2O^{2-}_{(ads)} \leftrightarrow H_2O + CO_2 + 4e^{-} \quad (5)$$

Therefore, the trapped electrons by the $O^{-}$ and $O^{2-}$ ions were released back into the conduction band of ZnO, which decreased the electron depletion layer, resulting in a low resistance state (Fig. 5b and 5d).

The sensing property was obtained from the resistance result, thus the gas response is defined as $\Delta R/R_g$, where $R_a$ and $R_g$ are the resistances in air and gas, respectively, and $\Delta R = |R_a - R_g|$ [1,41]. In the sensing response plots converted from Fig. 4 (Fig. S4a-e), we found two main results; dramatically different response has a laser power dependency and all sensor devices show the highest response result at an operating temperature of 400 °C. We understand the optimum temperature of 400 °C is the formaldehyde sensing operation for all sensors. This result is the same data with other types of ZnO-based formaldehyde sensors at the operating temperature of 400 °C [42]. In the representative plot of the chemiresistive variation at 400 °C in the laser power dependence (Fig. 6a), the 3 W laser-induced ZnO mesh sensor exhibited the highest sensing response with a ca. 6682.8 value, the sensor with the 4 W laser power condition represented a quite similar level to that of the 3 W system (response = 6234.6, and other responses are 386.4 for 0 W, 901.8 for 1 W, and 1687.6 for 2 W). Indeed, the higher laser power leads to a superior sensing response. In particular, at the 3 W or 4 W laser power condition, the response is extremely high value. It is because not only a more ideal ZnO crystal in the mesh structure that allows effective physical adsorption of formaldehyde including superior permeability via the few nanometer-sized pores but also a higher O-deficient level that generates more oxygen ion species interacting with formaldehyde. Most of all, at the high operating temperature, it is important to maintain the integrity of the structure to claim a relationship between the sensing response and morphological effect. We thereby investigated the variation of crystal phases of the laser power-dependent ZnO mesh structures at the temperature range of 300 – 500 °C (Fig. S5). We found that the ZnO crystal structure was kept, in particular at the laser power conditions over 2 W, and a trend of its crystallinity followed the crystal result at room temperature of Fig. 2f. From the results, we tentatively argue that the laser-induced ZnO mesh sensor showed an excellent sensing performance in the mesh structure formed as a precise ZnO crystal framework.

With the gas detection level, the transient response is another key parameter to determine the sensing ability of gas sensors. We focused on the sensing curves in the response results to understand the sensing transients for the response and recovery as a function of laser power. The response ($\tau_{res}$) and recovery ($\tau_{rec}$) time can be estimated as the time required to reach a 90 % resistance level when the device is exposed to formaldehyde and air, respectively [43]. The higher laser power even enables the ZnO mesh sensor to respond to faster adsorption of the formaldehyde, as follows in a sequence; $\tau_{res}$ is 0.98 s, 1.06 s, 2.96 s, 3.92 s, and 2.92 s for 4 W, 3 W, 2 W, 1 W, and 0 W condition, respectively (Fig. 6b). In particular, at the 4 W laser power condition, the sensor device exhibited ultra-fast response reactivity within 1 s. It is a considerably worthy result because the current state of formaldehyde sensors shows around 4 s in the $\tau_{res}$ time [44]. A considerably high surface area according to the mesh structure including few nanometer-sized pores allows tremendous formaldehyde molecules in

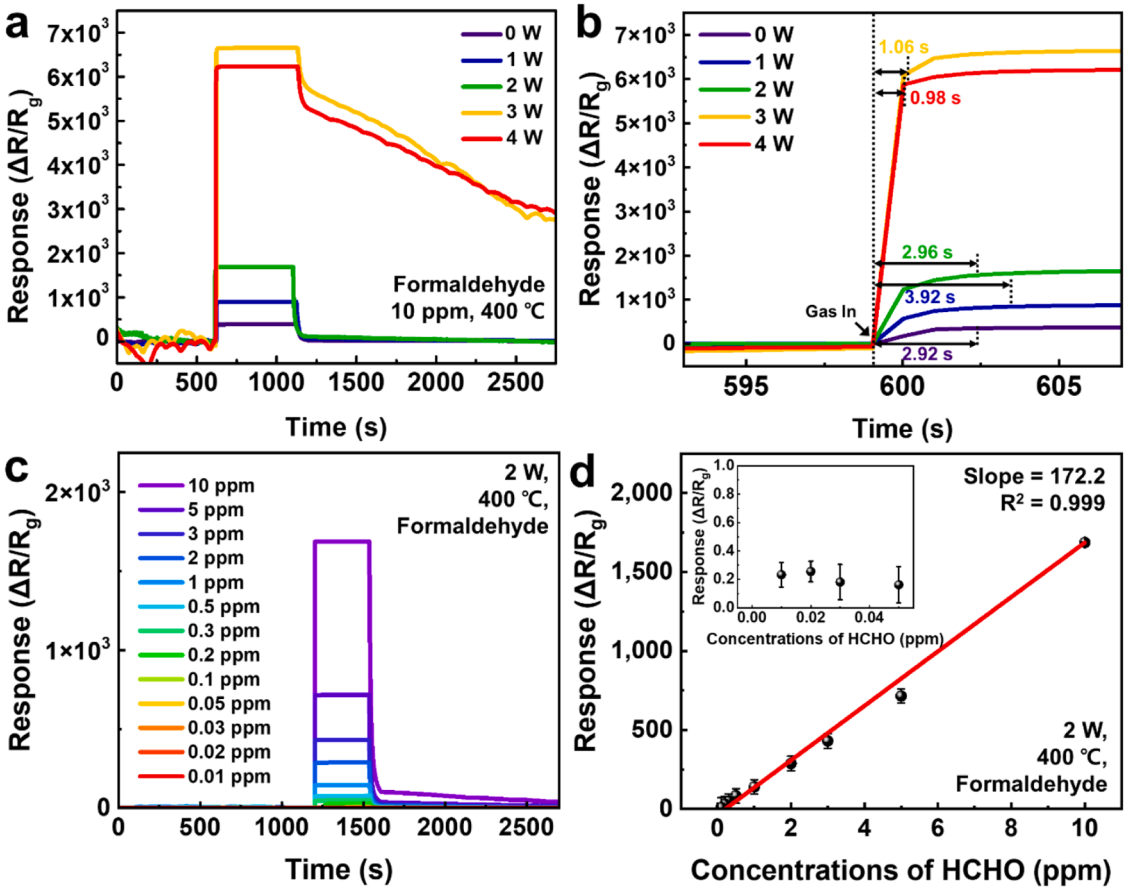


**Fig. 6.** (a) Representative plot of sensing responses for the laser power-dependent ZnO chemiresistive devices at an operating temperature of 400 °C. (b) Response time in sensing transients. (c) Formaldehyde concentration-dependent sensing responses in the 2 W- ZnO mesh sensor. (d) Corresponding to the sensitivity result with the slope of a linear fit.

the structure in a short time, leading the ultra-fast response time. For the $\tau_{rec}$ times, however, they show a different transient trend compared with the $\tau_{res}$. As shown in Fig. S4f, up to 2 W laser power condition, the recovery response revealed a similar $\tau_{rec}$ of ca. 46 s. In the sensor devices with higher laser power conditions of 3 W and 4 W (inset figure in Fig. S4f), slow gas desorption was observed.

Based on the $\tau_{rec}$ result including the $\tau_{res}$, we targeted the 2 W laser-induced ZnO mesh sensor that revealed sufficiently fast recovery performance. We thereby investigated the effect of formaldehyde sensitivity on the 2 W laser-induced ZnO mesh sensor. Fig. 6c displays the sensing responses depending on the formaldehyde concentration from 0.01–10 ppm at 400 °C. At the low concentration, i.e., under 0.1 ppm, the chemiresistive device sensitively detected formaldehyde gas, demonstrating that the 2 W laser-induced ZnO mesh sensor achieved a low detection limit (LOD) of ~ 0.1 ppm formaldehyde. This LOD is a quite similar level to the required value which is the World Health Organization (WHO), and thus the LOD is a significantly meaningful value in formaldehyde-based sensors. Furthermore, the sensor showed precisely concentration-dependent sensing performance. This result exhibited a linear relationship with a high linear correlation coefficient of $R^2 = 0.999$ as a function of formaldehyde concentration, resulting in an ultra-high sensitivity value of ca. 172.2 (a slope of the linear plot) (Fig. 6d). It means that depending on the formaldehyde concentration, formaldehyde molecules that are provided with a certain amount at each concentration totally reacted with adsorbed oxygen ions on/in the ZnO mesh structure.

Ultimately, the effect of the ZnO mesh structure that has few nanometer-sized pores is remarkable on the formaldehyde selectivity. We tested the sensing response for other target gases in the 2 W laser-induced ZnO mesh sensor at 400 °C (Fig. 7a). As investigated in Fig. 6, in the formaldehyde detection to 10 ppm, the 2 W laser sensor device showed a high response of 1687.6. In terms of the sensing response of the 3 W laser-induced ZnO mesh sensor, the response result is 6682.8. The response values in the detection of 10 ppm acetone and styrene showed 28.5 and 12.8, respectively, whereas responses to other gases such as $CO_2$, $NH_3$, $NO_2$, NO, acetaldehyde, and ethanol at the same concentration of 10 ppm were negligibly low (all gases are almost 0). This selectivity trend was also observed in the comparison result between 0 W and 2 W laser-induced ZnO mesh sensors (Fig. S6) and the operating temperature-dependent selectivity results (Fig. S7). The exclusive detection of formaldehyde (inset figure of Fig. 7a) is due to the design of the ZnO structure, specifically the mesh structure with few nanometer-sized pores. The sensing response is significantly influenced by the molecular size and dipole moment of the gas molecules. The molecular size of formaldehyde is 2.43 Å in kinetic diameter, while other target molecules show larger sizes: 4.69 Å for acetone, 3.34 Å for styrene, 3.26 Å for $NH_3$, 3.40 Å for $NO_2$, 5.10 Å for acetaldehyde, and 4.50 Å for ethanol. For the dipole moment (D), formaldehyde has a relatively high value of 2.30 D (acetone of 2.88 D, styrene of 0.13 D, $CO_2$ of 0 D, $NH_3$ of 1.46 D, $NO_2$ of 0.63 D, acetaldehyde of 2.69 D, and ethanol of 1.69 D) [45]. The tiny size and large D value of formaldehyde enable effective chemical adsorption on the mesh structure and good permeability through the few nanometer-sized pores. This exclusive selectivity for formaldehyde can be attributed to several factors. Chemical interaction plays a crucial role, as the unique molecular structure of formaldehyde allows for stronger interactions with the ZnO surface compared to larger molecules, enhancing both adsorption capacity and sensitivity. Additionally, formaldehyde may require lower activation energy for effective adsorption on the ZnO mesh structure, facilitating detection even at low concentrations and contributing to the observed high response levels. Furthermore, the presence of oxygen vacancies on the ZnO surface is critical for enhancing selectivity. These vacancies can interact favorably with formaldehyde, enabling a more efficient detection mechanism. The ultra-exclusive selectivity of formaldehyde in the laser-induced ZnO mesh sensor stands out when compared to previously reported results (Fig. 7b) [46–65]. Most formaldehyde gas sensors have shown sensing responses between 0 and 20 as a function of formaldehyde concentration, from 0.05 ppm to 10 ppm. The maximum response of approximately 52.5 was observed in reference [58] for formaldehyde detection at 10 ppm concentration. In a more specific category, our

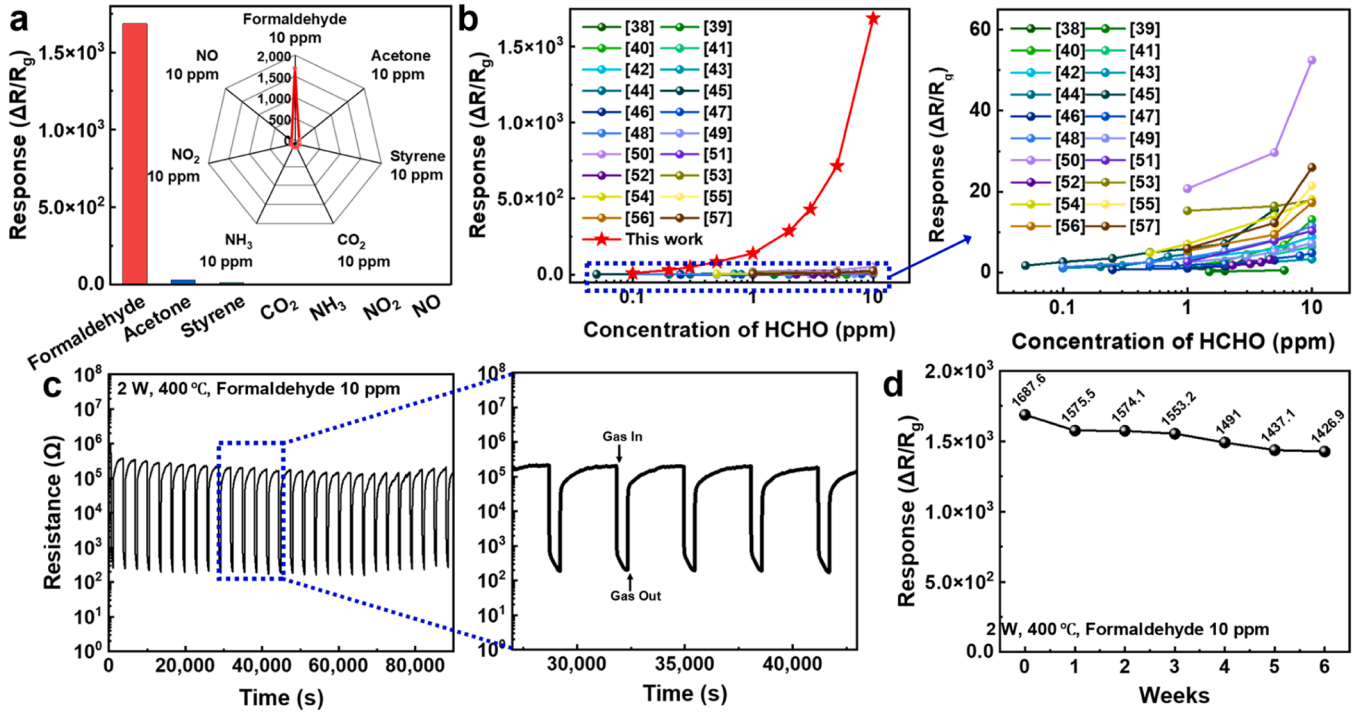


**Fig. 7.** (a) Gas responses toward various test gases for the 2 W laser-induced ZnO mesh sensor in a 400 °C condition. (b) Comparison of sensing response of the laser-induced ZnO mesh sensor to previously reported formaldehyde gas sensors (references were highlighted as a dashed blue box). (c) Repeated sensing transients (40 cycles), and the blue dash square shows a highlighted curve of real-time 5-cycle resistance. (d) Long-term stability in the sensing performance.

laser-induced ZnO mesh sensor showed an extremely high sensing response, even at low concentrations of formaldehyde [54,57,64, 66–69].

In terms of stability in the sensing performance, the 2 W laser-induced ZnO mesh sensor showed an excellent stable chemiresistive device. We tested the sensor device for the detection of 10 ppm formaldehyde with 40 cycles at 400 ℃. Fig. 7c exhibited a considerably constant resistance result in the gas-in and out system, which is confirmed in the magnified plot of the real-time resistance curves with a highlight of 5 cycles (dash blue box) in detail. Fig. 7d represents the long-term stability of the sensor device when exposed to 10 ppm formaldehyde at 400 °C for 7 weeks. During the sensing period under the high operating temperature, the sensing response value was only changed with a ~ 15 % reduction level.

## 4. Conclusions

In this work, we designed a formaldehyde gas sensor that exhibits ultra-exclusive selectivity based on a ZnO mesh structure. $CO_2$ laser irradiation enabled the rapid fabrication of the ZnO mesh structure within 1 min, forming few nanometer-sized pores between ZnO crystal domains. With increasing laser power, particularly at 3 W and 4 W, the ZnO crystals were precisely synthesized, and smaller pores under 9 nm were formed, which enhanced gas permeability and adsorption. Furthermore, more oxygen vacancies were generated in the ZnO crystal framework, reaching up to 38 % at 4 W, significantly contributing to the sensor's selectivity and sensitivity. This unique structure allowed for efficient chemical interaction between formaldehyde and the oxygen ion species on the surface of ZnO crystals. As a result, the 3 W laser-induced ZnO mesh sensor achieved an exceptional sensing response of over 6682 and an ultra-fast response time of 0.98 s, demonstrating superior performance in formaldehyde detection. In terms of recovery time, the 2 W laser-induced ZnO mesh sensor exhibited a response value of 1687.6 with a low detection limit of $< 0.1$ ppm, meeting the requirements for detecting trace formaldehyde concentrations in real-world environments. Moreover, the sensor exhibited remarkable long-term stability, with only a 15 % reduction in performance after 7 weeks of continuous operation at 400°C, confirming its durability. The combination of fast response, high selectivity, low detection limit, and long-term reliability makes this performance an overwhelming advancement in the field of formaldehyde gas sensors. Therefore, our ZnO mesh structure with few nanometer-sized pores offers a promising strategy for developing high-performance formaldehyde sensors, with significant potential for indoor and outdoor air monitoring.

## CRediT authorship contribution statement

**Jihyun Lee:** Formal analysis, Data curation, Conceptualization. **SeungJo Kang:** Writing – review & editing, Writing – original draft, Methodology, Investigation. **YuJin Kim:** Writing – review & editing, Writing – original draft, Validation, Investigation, Formal analysis, Data curation. **James Jungho Pak:** Validation, Resources. **Wooyoung Lee:** Validation, Supervision, Project administration, Funding acquisition.

## Declaration of Competing Interest

The authors declare no competing financial interest.

## Acknowledgments

This research was supported by the National Research Foundation of Korea (NRF) grant funded by the Korean government (MIST) (No. NRF-2022M3H4A3053304, National Core Materials Research Center, Platform Type) and the Technology Innovation Program (20013621) under the Center for Super Critical Material Industrial Technology funded by the Ministry of Trade, Industry & Energy (MOTIE, Korea), as well as Research and Development Program under the National Fire Agency (RS-2024-00404040) funded by Ministry of the Interior and Safety of Korea (MOIS, Korea).

## Appendix A. Supporting information

Supplementary data associated with this article can be found in the online version at doi:10.1016/j.jallcom.2025.178475.

## Data availability

Data will be made available on request.

## References

[1] Y.K. Jo, S.-Y. Jeong, Y.K. Moon, Y.-M. Jo, J.-W. Yoon, J.-H. Lee, Exclusive and ultrasensitive detection of formaldehyde at room temperature using a flexible and monolithic chemiresistive sensor, Nat. Commun. 4 (2021) 4955.
[2] C. Umansky, A.E. Morellato, L.B. Pontel, Illuminating cellular formaldehyde, Nat. Commun. 12 (2021) 580.
[3] R. Prajesh, V. Goyal, M. Nahid, V. Saini, A.K. Singh, A.K. Sharma, J. Bhargava, A. Agarwal, Nickel oxide (NiO) thin film optimization by reactive sputtering for highly sensitive formaldehyde sensing, Sens. Actuators B Chem. 318 (2020) 128166.
[4] H. Tian, H. Fan, M. Li, L. Ma, Zeolitic imidazolate framework coated ZnO nanorods as molecular sieving to improve selectivity of formaldehyde gas sensor, ACS Sens 1 (2016) 243.
[5] T. Zhou, T. Zhang, Recent progress of nanostructured sensing materials from 0D to 3D:overview of structure-property-application relationship for gas sensor, Small Methods 5 (2021) 2100515.
[6] S.M. Majhi, H.-J. Lee, H.-N. Choi, H.-Y. Cho, J.-S. Kim, C.-R. Lee, Y.-T. Yu, Construction of novel hybrid PdO-ZnO p-n heterojunction nanostructures as a high-response sensor for acetaldehyde gas, CrystEngComm 21 (2019) 5084.
[7] S.-Y. Tang, C.-C. Yang, T.-Y. Su, T.-Y. Yang, S.-C. Wu, Y.-C. Hsu, Y.-Z. Chen, T.-N. Lin, J.-L. Shen, H.-N. Lin, P.-W. Chiu, H.-C. Kuo, Y.-L. Chueh, Design of core-shell quantum dots – 3D WS 2 nanowall hybrid nanostructures with high-performance bifunctional sensing applications, ACS Nano 14 (2020) 12668.
[8] Y. Li, Z. Song, Y. Li, S. Chen, S. Li, Y. Li, H. Wang, Z. Wang, Hierarchical hollow MoS 2 microspheres as materials for conductometric $NO_2$ gas sensors, Sens. Actuators B Chem. 282 (2019) 259.
[9] S.M. Majhi, A. Mirzaei, H.W. Kim, S.S. Kim, T.W. Kim, Recent advances in energysaving chemiresistive gas sensors: a review, Nano Energy 79 (2021) 105369.
[10] K.-R. Park, H.-B. Cho, J. Lee, Y. Song, W.-B. Kim, Y.-H. Choa, Design of highly porous $SnO^{2-}$CuO nanotubes for enhancing H 2S gas sensor performance, Sens. Actuators B Chem. 302 (2020) 127179.
[11] T. Ma, L. Zheng, Y. Zhao, Y. Xu, J. Zhang, X. Liu, Highly porous double-shelled hollow hematite nanoparticles for gas sensing, ACS Appl. Nano Mater. 2 (2019) 2347.
[12] M. Lee, H.-S. Lee, M.Y. Kim, K.H. Lee, W. Lee, Significant improvement in the acetone sensing performance of Ag-decorated ZnO porous nanosheets through defect engineering by Li˙ion implantation, Sens. Actuators B Chem. 372 (2022) 132671.
[13] H.G. Moon, Y.-S. Shim, D. Su, H.-H. Park, S.-J. Yoon, H.W. Jang, Embossed $TiO_2$ thin films with tailored links between hollow hemispheres: synthesis and gas-sensing properties, J. Phys. Chem. C 115 (2011) 9993.
[14] M. AI-Hashem, S. Akbar, P. Morris, Role of oxygen vacancies in nanostructured metaloxide gas sensors: a review, Sens. Actuators B Chem. 301 (2019) 126845.
[15] D. Liu, J. Wan, H. Wang, G. Pang, Z. Tang, Mesoporous Au@ZnO flower-like nanostructure for enhanced formaldehyde sensing performance, Inorg. Chem. Commun. 102 (2019) 203.
[16] S. Wang, F. Jia, X. Wang, L. Hu, Y. Sun, G. Yin, T. Zhou, Z. Feng, P. Kumar, B. Liu, Fabrication of ZnO nanoparticles modified by uniformly dispersed Ag nanoparticles: enhancement of gas sensing performance, ACS Omega 5 (2020) 5209.
[17] Y. Yang, S. Wu, Y. Cao, S. Li, T. Xie, Y. Lin, Z. Li, A highly efficient room-temperature formaldehyde gas sensor based on a Ni-doped ZnO hierarchical porous structure decorated with NiS illuminated by UV light, J. Alloy. Compd. 920 (2022) 165850.
[18] K. Khojier, Preparation and investigation of Al-doped ZnO thin films as a formaldehyde sensor with extremely low detection limit and considering the effect of RH, Mater. Sci. Semicond. 121 (2021) 105283.
[19] X. Li, N. Zhang, C. Liu, S. Adimi, J. Zhou, D. Liu, S. Ruan, Enhanced gas sensing properties for formaldehyde based on ZnO/Zn2SnO4 composites from one-step hydrothermal synthesis, J. Alloy. Compd. 850 (2021) 156606.
[20] X. Xing, Y. Yang, Z. Yan, Y. Hu, T. Zou, Z. Wang, Y. Wang, CdO-Ag-ZnO nanocomposites with hierarchically porous structure for effective VOCs gas-sensing properties, Ceram. Int. 45 (2019) 4322.
[21] H. Tai, X. Li, Y. Jiang, G. Xie, X. Du, The enhanced formaldehyde-sensing properties of P3HT-ZnO hybrid thin film OTFT sensor and further insight into its stability, Sensors 15 (2015) 2086.
[22] B. Zhang, J. Wang, Q. Wei, P. Yu, S. Zhang, Y. Xu, Y. Dong, Y. Ni, J. Ao, Y. Xia, Visible light-induced room-temperature formaldehyde gas sensor based on porous

three-dimensional ZnO nanorod clusters with rich oxygen vacancies, ACS Omega 7 (2022) 22861.
[23] H. Chen, C. Li, X. Zhang, W. Yang, ZnO nanoplates with abundant porosity for significant formaldehyde-sensing, Mater. Lett. 260 (2020) 126982.
[24] B.Y. Park, R. Zaouk, M.J. Madou, Fabrication of microelectrodes using the lift-off technique, Methods Mol. Biol. 321 (2006) 23.
[25] D. Ju, H. Xu, J. Zhang, J. Guo, B. Cao, Direct hydrothermal growth of ZnO nanosheets on electrode for ethanol sensing, Sens. Actuators B Chem. 201 (2014) 444.
[26] W. Zhang, Y. Lei, Q. Jiang, F. Ming, P.M.F.J. Costa, H.N. Alshareef, 3D laser scribed graphene derived from carbon nanospheres: an ultrahigh-power electrode for supercapacitors, Small, Methods 3 (2019) 190005.
[27] A.K. Thakur, B. Lin, F.H. Nowrin, M. Malmali, Comparing structure and sorption characteristics of laser-induced graphene (LIG) from various polymeric substrates, ACS EST Water 2 (2022) 75.
[28] C. Zhang, G. Liu, X. Geng, K. Wu, M. Debliquy, Metal oxide semiconductors with highly concentrated oxygen vacancies for gas sensing materials: a review, Sens. Actuator A Phys. 309 (2020) 112026.
[29] H. Yuan, S.A.A.A. Aljneibi, J. Yuan, Y. Wang, H. Liu, J. Fang, C. Tang, X. Yan, H. Cai, Y. Gu, S.J. Pennycook, J. Tao, D. Zhao, ZnO nanosheets abundant in oxygen vacancies derived from metal-organic frameworks for ppb-level gas sensing, Adv. Mater. 31 (2019) 1807161.
[30] J.M. Walker, S.A. Akbar, P.A. Morris, Synergistic effects in gas sensing semiconducting oxide nano-heterostructures: a review, Sens. Actuators B Chem. 286 (2019) 624.
[31] H. Ji, W. Zeng, Y. Li, Gas sensing mechanisms of metal oxide semiconductors: a focus review, Nanoscale 11 (2019) 22664.
[32] J. Zhuang, S. Weng, W. Dai, P. Liu, Q. Liu, Effects of interface defects on charge transfer and photoinduced properties of $TiO_2$ bliayer films, J. Phys. Chem. C 116 (2012) 25354–25361.
[33] H. Liu, H.T. Ma, X.Z. Li, W.Z. Li, M. Wu, X.H. Bao, The enhancement of $TiO_2$ photocatalytic activity by hydrogen thermal treatment, Chemosphere 50 (2003) 39–46.
[34] H. Bai, Z. Liu, D.D. Sun, Hierarchical ZnO/Cu "corn-like" materials with high photodegradation and antibacterial capability under visible light, Phys. Chem. Chem. Phys. 13 (2011) 6205–6210.
[35] N.V. Duy, N.X. Thai, T.M. Ngoc, D.T.T. Le, C.M. Hung, H. Nguyen, M. Tonezzer, N. V. Hieu, N.D. Hoa, Design and fabrication of effective gradient temperature sensor array based on bilayer $SnO_2$/Pt for gas classification, Sens. Actuators B Chem. 351 (2022) 130979.
[36] K. Chen, Y. Zhou, R. Jin, T. Wang, F. Liu, C. Wang, X. Yan, P. Sun, G. Lu, Gas sensor based on cobalt-doped 3D inverse opal $SnO_2$ for air quality monitoring, Sens. Actuators B Chem. 350 (2022) 130807.
[37] C. Jin, M.S. Choi, K.H. Lee, S.-W. Choi, Gas sensing behavior of p-NiO/n-ZnO composite nanofibers depending on varying p-NiO content: selectivity and humidityindependence for oxidizing and reducing gas molecules, Sens. Actuators B Chem. 349 (2021) 130813.
[38] N. Goel, K. Kunal, A. Kushwaha, M. Kumar, Metal oxide semiconductors for gas sensing, Eng. Rep. (2022) e12604.
[39] C. Xiao, Z. Tang, Z. Ma, X. Gao, H. Wang, L. Jia, High performance porous LaFeO 3 gas sensor with embedded p-n junctions enabling ppb-level formaldehyde detection, Sens. Actuators B Chem. 397 (2023) 134670.
[40] W. Guo, B. Zhao, Q. Zhou, Y. He, Z. Wang, N. Radacsi, Fe-doped ZnO/reduced graphene oxide nanocomposite with synergic enhanced gas sensing performance for the effective detection of formaldehyde, ACS Omega 4 (2019) 10252.
[41] F.E. Annanouch, A. Alagh, P. Umek, J. Casanova-Chafer, C. Bittencourt, E. Llobet, Controlled growth of 3D assemblies of edge enriched multilayer MoS2 nanosheets for dually selective NH3 and NO2 gas sensors, J. Mater. Chem. C 10 (2022) 11027.
[42] S. Crispi, G. Neri, Development of a conductometric sensor based on Al, Ca-doped ZnO for the detection of formaldehyde, Sensors 22 (2022) 7465.
[43] K. Kim, P.G. Choi, T. Itoh, Y. Masuda, Effect of coordinatively unsaturated sites in MOFderived highly porous CuO for catalyst-free ppb-level gas sensors, Adv. Mater. Interfaces 8 (2021) 2100283.
[44] S. Das, S. Kumar, J. Singh, M. Kumar, Decoration of laser-ablated ZnO nanoparticles over sputtered deposited $SnO_2$ thin film based formaldehyde sensor, Sens. Actuators B Chem. 367 (2022) 132114.
[45] A. Kumar, W.J. Meath, Isotropic dipole properties for acetone, acetaldehyde and formaldehyde, Mol. Phys. 90 (1997) 389.
[46] X. Fu, P. Yang, X. Xiao, D. Zhou, R. Huang, X. Zhang, F. Cao, J. Xiong, Y. Hu, Y. Tu, Y. Zou, Z. Wang, H. Gu, Ultra-fast and highly selective room-temperature formaldehyde gas sensing of Pt-decorated $MoO_3$ nanobelts, J. Alloy. Compd. 797 (2019) 666.
[47] L.-Y. Zhu, K. Yuan, J.-G. Yang, H.-P. Ma, T. Wang, X.-M. Ji, J.-J. Feng, A. Devi, H.-L. Lu, Fabrication of heterostructured p-CuO/n-$SnO_2$ core-shell nanowires for enhanced sensitive and selective formaldehyde detection, Sens. Actuators B Chem. 290 (2019) 233.
[48] D. Liu, J. Pan, J. Tang, W. Liu, S. Bai, R. Luo, Ag decorated $SnO_2$ nanoparticles to enhance formaldehyde sensing properties, J. Phys. Chem. Solids 124 (2019) 36.
[49] J. Cao, N. Zhang, S. Wang, H. Zhang, Electronic structure-dependent formaldehyde gas sensing performance of the $In_2O_3/Co_3O_4$ core/shell hierarchical heterostructure sensors, J. Colloid Interface Sci. 577 (2020) 19.
[50] L. Huang, Z. Fan, X. Li, S. Wang, W. Guo, Facile synthesis of CaFe 2O 4 nanocubes for formaldehyde sensor, Mater. Lett. 288 (2021) 129351.
[51] K. Zhu, S. Ma, Y. Tie, Q. Zhang, W. Wang, S. Pei, X. Xu, Highly sensitive formaldehyde gas sensors based on Y-doped $SnO_2$ hierarchical flower-shaped nanostructures, J. Alloy. Compd. 792 (2019) 938.
[52] Y. Xu, X. Tian, Y. Fan, Y. Sun, A formaldehyde gas sensor with improved gas response and sub-ppm level detection limit based on NiO/NiFe 2O 4 composite nanotetrahedrons, Sens. Actuators B Chem. 309 (2020) 127719.
[53] T. Wang, B. Jiang, Q. Yu, X. Kou, P. Sun, F. Liu, H. Lu, X. Yan, G. Lu, Realizing the control of electronic energy level structure and gas-sensing selectivity over heteroatom-doped $In_2O_3$ spheres with an inverse opal microstructure, ACS Appl. Mater. Interfaces 11 (2019) 9600.
[54] S. Das, S. Kumar, J. Singh, M. Kumar, Decoration of laser-ablated ZnO nanoparticles over sputtered deposited $SnO_2$ thin film based formaldehyde sensor, Sens. Actuators B Chem. 367 (2022) 132114.
[55] N. Zhang, Y. Lu, Y. Fan, J. Zhou, X. Li, S. Adimi, C. Liu, S. Ruan, Metal–organic framework-derived ZnO/$ZnCo_2O_4$ microspheres modified by catalytic PdO nanoparticles for sub-ppm-level formaldehyde detection, Sens. Actuators B Chem. 315 (2020) 128118.
[56] G. Liu, M. Zhang, B. Wu, Y. Zhuang, R. Ramachandran, C. Zhao, F. Wang, Nanocomposites of pre-oxidized Ti3C2Tx MXene and $SnO_2$ nanosheets for highly sensitive and stable formaldehyde gas sensor, Ceram. Int. 49 (2023) 2583.
[57] B. Li, H. Liu, Q. Zeng, S. Dong, W. Feng, Hierarchical porous NiO doped ZnO nanocomposite for formaldehyde gas sensor with high sensitivity, fast response/recovery and good selectivity, Surf. Interfaces 36 (2023) 102502.
[58] Y. Wu, S. Zhang, Q. Rong, D. Xie, Y. Zhang, Q. Liu, J. Zhang, Rice-grain $Sm_2O_3$/$SmFeO_3$ nanoparticles as high selectivity formaldehyde gas sensor prepared by precipitation, Mater. Lett. 292 (2021) 129416.
[59] Y. Bian, L. Nie, A. Wang, L. Zhang, R. Yue, N. Han, Y. Chen, Facile synthesis of stoichiometric InOCl mesoporous material for high performance formaldehyde gas sensors, Sens. Actuators B Chem. 319 (2020) 128078.
[60] Y. Tie, S.Y. Ma, G.J. Yang, Q. Chen, S.T. Pei, L. Ma, W.Q. Wang, K.M. Zhu, Q. X. Zhang, O. Almamoun, Improved formaldehyde sensor of $Zn_2SnO_4/SnO_2$ microcubes by compositional evolution and Y 2O 3 decoration, Ceram. Int. 45 (2019) 5384.
[61] R. Zhao, X. Zhang, S. Peng, P. Hong, T. Zou, Z. Wang, X. Xing, Y. Yang, Y. Wang, Shaddock peels as bio-templates synthesis of Cd-doped $SnO_2$ nanofibers: a high performance formaldehyde sensing material, J. Alloy. Compd. 813 (2020) 152170.
[62] D. Wang, K. Wan, M. Zhang, H. Li, P. Wang, X. Wang, J. Yang, Constructing hierarchical $SnO_2$ nanofiber/nanosheets for efficient formaldehyde detection, Sens. Actuators B Chem. 283 (2019) 714.
[63] R. Zhang, S.Y. Ma, Q.X. Zhang, K.M. Zhu, Y. Tie, S.T. Pei, B.J. Wang, J.L. Zhang, Highly sensitive formaldehyde gas sensors based on Ag doped $Zn_2SnO_4/SnO_2$ hollow nanospheres, Mater. Lett. 254 (2019) 178.
[64] J. Huang, H. Liang, J. Ye, D. Jiang, Y. Sun, X. Li, Y. Geng, J. Wang, Z. Qian, Y. Du, Ultrasensitive formaldehyde gas sensor based on Au-loaded ZnO nanorod arrays at low temperature, Sens. Actuators B Chem. 346 (2021) 130568.
[65] R. Xu, L.-X. Zhang, M.-W. Li, Y.-Y. Yin, J. Yin, M.-Y. Zhu, J.-J. Chen, Y. Wang, L.-J. Bie, Ultrathin $SnO_2$ nanosheets with dominant high-energy {001} facets for low temperature formaldehyde gas sensor, Sens. Actuators B Chem. 289 (2019) 186.
[66] Y. Zhang, M. Wang, X. San, L. Zhang, N. Wang, G. Wang, D. Meng, Y. Shen, Highly selective gas sensors for formaldehyde detection based on ZnO@ZIF-8 core-shell heterostructures, Sens. Actuators B Chem. 398 (2024) 134689.
[67] K.S. Varshini, K.R. Kishore, B.G. Jeyaprakash, D. Balamurugan, Heterostructured ZnO/Fe 2O 3 nanograins-based sensors for formaldehyde detection, J. Mater. Sci. Mater. Electron. 34 (2023) 1317.
[68] F. Xu, W. Li, S. Sun, A. Zhong, X. Cheng, J. Shi, Z. Li, J. Li, W. Zhang, X. Wang, Y. Ma, A.H.-P. Ho, Expanding selectivity functionality of a ZnO nanotetrapod-based volatile organic compound sensor using Au nanoparticle decoration, ACS Appl. Nano Mater. 6 (2023) 8335.
[69] M. Sinha, S. Neogi, R. Ghosh, Temperature dependent selectivity switching from methanol to formaldehyde using ZnO nanorod based chemiresistive sensor, Sens. Actuators A Phys. 357 (2023) 114405.